ELSEVIER

International Journal of Refrigeration 27 (2004) 302–308

INTERNATIONAL JOURNAL OF refrigeration

www.elsevier.com/locate/ijrefrig

Three-dimensional measurement of ice crystals in frozen dilute solution

Shigeaki Ueno[a], Gab-Soo Do[a], Yasuyuki Sagara[a,*], Ken-ichi Kudoh[b], Toshiro Higuchi[b]

[a]*Department of Global Agricultural Sciences, Graduate School of Agricultural and Life Sciences, The University of Tokyo, 1-1-1 Yayoi, Bunkyo-ku, Tokyo 113-8657, Japan*

[b]*Department of Precision Machinery Engineering, Graduate School of Engineering, The University of Tokyo, 7-3-1 Hongo, Bunkyo-ku, Tokyo 113-8658, Japan*

Received 7 October 2002; received in revised form 17 February 2003; accepted 11 March 2003

Abstract

A Micro-Slicer Image Processing System (MSIPS) has been applied to observe the ice crystal structures formed in frozen dilute solutions. Several characteristic parameters were also proposed to investigate the three-dimensional (3-D) morphology and distribution of ice crystals, based on their reconstructed images obtained by multi-slicing a frozen sample with the thickness of 5 μm. The values of characteristic parameters were determined for the sample images with the dimension of 530×700×1000 μm. The 3-D morphology of ice crystals was found to be a bundle of continuous or dendrite columns at any freezing condition. The equivalent diameter of ice crystals were in the range of 73–169 μm, and decreased exponentially with increasing freezing rate at the copper cooling plate temperature of −20 to −80 °C. At the T_{cp} −40 °C, the volumes of ice crystals were in the range of 4.6×10^4 μm^3 to 3.3×10^7 μm^3, and 36 ice columns were counted in the 3-D image.

Keywords: Solution; Freezing; Ice; Crystal; Formation; Optical system

Cristaux de glace dans des solutions diluées congelées : mesures en trois dimensions

Mots clés : Solution ; Congélation ; Glace ; Cristal ; Formation ; Optique

1. Introduction

Freezing operations have been used as food processing technologies such as freeze concentration, freeze-drying, freeze smashing and freeze texturization. Since water is the primary component of foods, freezing of food involves the phase change of water to ice. The morphology, size and distribution of ice crystals formed during the freezing process of foods are fundamental information to design both commercial plant operations as well as the quality of final products [1–7].

Observation of ice crystals may be direct or indirect. Direct observation methods include cryo-scanning electron microscopy [7], cold microscopy [8–10] and confocal

* Corresponding author. Tel.: +81-3-5841-7536; fax: +81-3-5841-5335.

E-mail address: asagara@mail.ecc.u-tokyo.ac.jp (Y. Sagara).

0140-7007/03/$35.00
doi:10.1016/S0140-7007(03)00043-4

Nomenclature

T_{cp}	copper cooling plate temperature, °C
R	freezing rate, °C h^{-1}
d	ice crystal diameter, μm
ML	ice crystal major length (major axis), μm
MW	ice crystal minor width (minor axis), μm
q	heat flux, J m^{-2} s
V	volume, μm^3

laser scanning microscopy [11]. These methods are used at a temperature below 0 °C by observing ice crystals directly. Indirect methods such as freeze substitution [1,12–15], freeze fixation [16] and freeze-drying techniques [17–21] are based on the hypothesis that the original ice crystal morphology is maintained after substitution and sublimation. However, these techniques still have disadvantages, because the microstructures would have changed in the vicinity of the sublimination process.

Faydi et al. [21] developed a direct observation method of ice crystals based on optical microscopy with episcopic coaxial lighting. They observed ice crystals in the cold room of −20 °C, and structural discrepancies were demonstrated between direct and indirect methods. Their result indicated that conventional freeze-drying method was inferior to direct methods, because of difficulty in maintaining the original structure of ice crystals.

Furthermore, although it is valuable to apply all these methods for two-dimensional or cross-sectional characteristics such as ice crystal size and distribution, the 3-D morphology of ice crystals is still unable to analyze quantitatively. Thus a micro-slicer image processing system (MSIPS) was developed to reconstruct 3-D internal images of biomaterials [22]. Do et al. [23] measured the surface area and volume of a sample of broccoli with the MSIPS. Yokota et al. [24,25] and Ogawa et al. [26] applied 3-D internal structure microscopy to observe the internal structure of several histological biomaterials and vegetables.

The objectives of the study were to develop a novel technique to observe and reconstruct 3-D images of ice crystals and to investigate the effects of freezing conditions on ice crystal size, morphology, volume and distribution of the ice crystals formed in frozen dilute solution.

2. Experimental apparatus and procedure

Two types of freezers were prepared for one-dimensional freezing of the samples. Fig. 1 shows a schematic diagram of program freezer (TNP87S, Nihon freezer, Japan). It is composed of a freezer, temperature controller, liquid nitrogen container and a thermo-recorder. A copper cooling plate was located on the top of the freezer and its surface temperature T_{cp} was controllable by using an electric heater and a flow rate regulator of liquid nitrogen in the range of room temperature to −150 °C. For more rapid freezing, a similar liquid nitrogen freezer was employed and its cooling plate temperature was controlled at −190 °C.

The sample holder was placed on the copper cooling plate equipped on the freezer as shown in Fig. 2. The holder is a cylindrical paraffin vessel of 8 mm in diameter and 30 mm in height and surrounded by heat insulator for accomplishing one-dimensional freezing. Temperature distribution of the sample was measured by using needle-type thermocouple probes of 0.3 mm in diameter made of copper-constantan wires and the changes in temperatures were monitored with a data acquisition system (MV100 Thermo recorder, Yokogawa Electric Co., Japan).

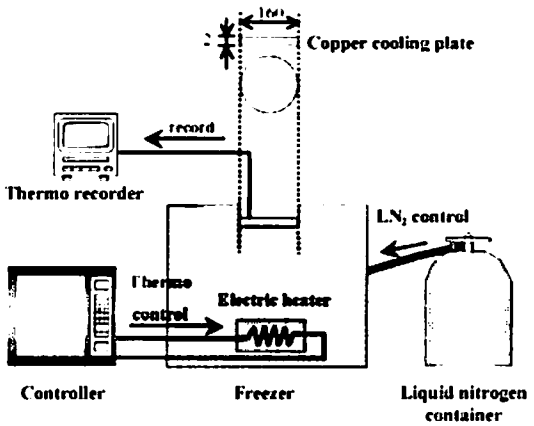

Fig. 1. Schematic diagram of program freezer.

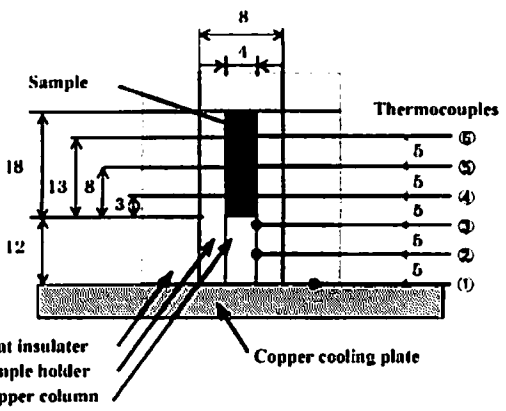

Fig. 2. Sample holder for the measuring of the sample temperature during freezing.

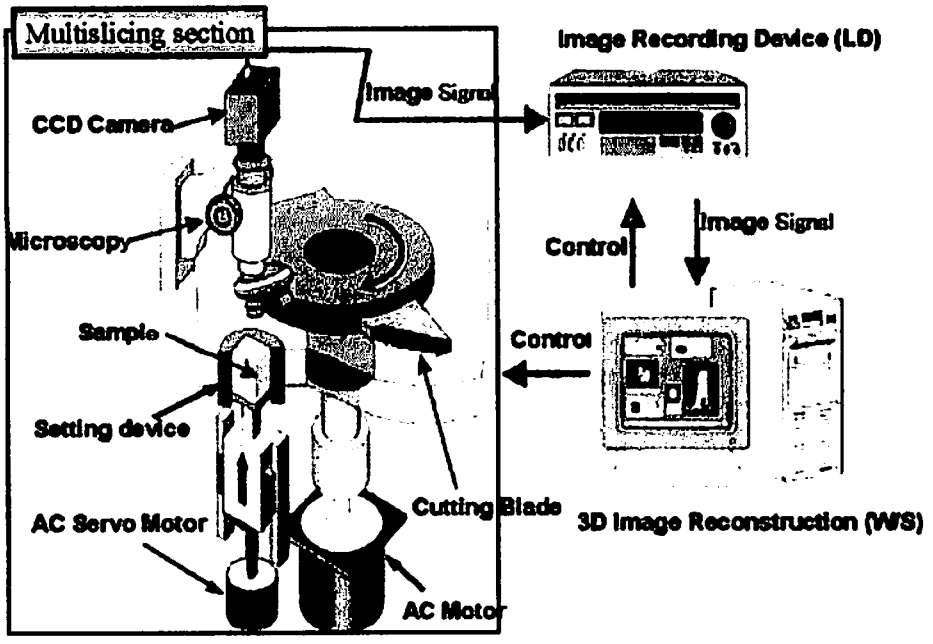

Fig. 3. Micro-slicer image processing system.

The MSIPS [22–25,27] is composed of a multi-slicing section to expose the cross-sections of a sample, an observation section and an imaging section as shown in Fig. 3. The cross-sectional images of exposed surfaces after slicing were captured directly with a CCD camera (DX930, Sony, Japan) through a fluorescent microscope (BX-FLA, Olympus, Japan), and recorded into a laser videodisc (LVR-300AN, Sony, Japan). The multi-slicing section was maintained at −40 °C with an immersion cooler during observation [27].

To prepare the sample solution, fluorescent Rhodamine B ($C_{28}H_{31}ClN_2O_3$) and agar were dissolved into hot distilled water. Final solute content of Rhodamine B and agar were in the range of 0.02–0.1 and 0.5–1.0 wt.%, respectively.

The copper column located at the lower part of the holder was used to determine the heat flux across the bottom sample surface during freezing. The solution was poured onto a copper column in the sample holder. When the sample was cooled down to room temperature, it was located on the copper cooling plate of the freezer. The temperature of the copper cooling plate was controlled according the freezing condition for each sample, and then one-dimensional freezing was carried out. After freezing, the sample holder was moved into the setting device of the MSIPS. The sample was continuously pushed up by the AC servo motor and sliced together with the paraffin sample holder at the revolution rate of 60 rpm with the thickness of 5 μm. The images of 3600 cross-sections were serially obtained per sample. The recorded 2-D images had 256 gray level with the resolution of 640×480 pixels (1 pixel = 1.1 μm). The 3-D image was reconstructed based on the volume rendering method by utilizing 3-D visualization software (AVS Express, Advanced Visual System Inc., USA) and displayed the internal structure as well as an arbitrary cross-section of the sample choosing observation angles.

The morphology of ice crystals was analyzed by the image analysis software (SPICCA II TVIP-5100, Nippon Avionics, Japan). The procedure of image analysis is shown as a flow diagram in Fig. 4. Captured images

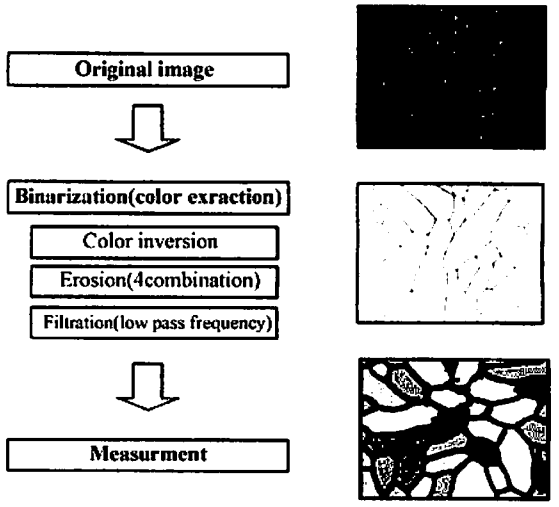

Fig. 4. Flow diagram of image analysis.

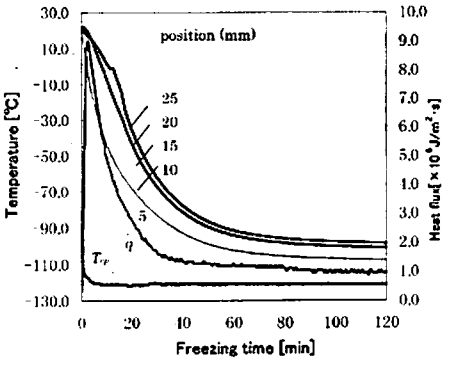

Fig. 5. Freezing curve at T_{cp} −120 °C.

were binarized and modified by means of inversion, erosion and low pass frequency filtration. Each of the ice crystals is individually labeled and their characteristic parameters are analyzed. The major length (ML), minor width (MW) and the equivalent diameter of ice crystal area (d) were measured and their ratio (ML/MW) was determined as an index of morphology. The volumes of ice columns were also analyzed by a volume analysis software (TRI 3D volume, Ratoc System Engineering Co. Ltd., Japan).

3. Results and discussion

In this section, the typical results obtained were presented for the samples having solute contents of 0.1 wt.% Rhodamine B and 1.0 wt.% of agar, respectively.

Freezing time and freezing rate (R) were calculated from the freezing curves that passed through a zone of maximum ice crystal formation for water. Fig. 5 shows the freezing curves obtained at T_{cp} −120 °C at various locations of thermocouples. Heat flux ($\dot{q}$) was calculated from both the temperature gradient monitored and thermal conductivity of a copper column. As shown in Fig. 5, the final temperature of sample at the distance of 8 mm from the bottom surface was −101.5 °C, and then

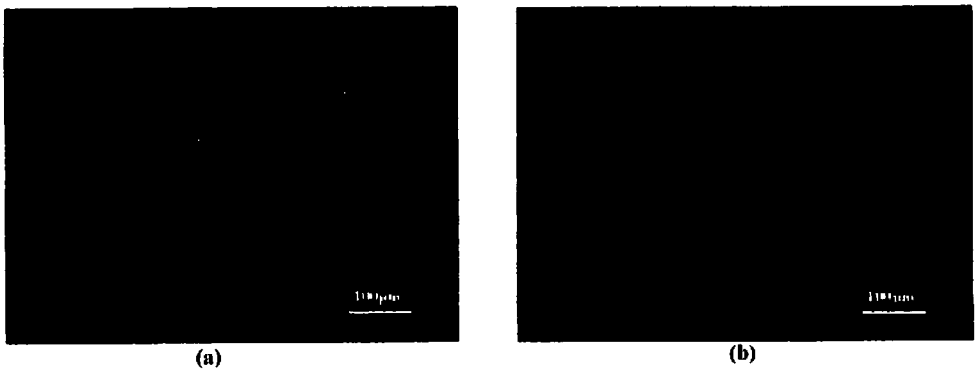

Fig. 6. Cross-section of ice crystals at T_{cp} −30 °C (a) and −190 °C (b).

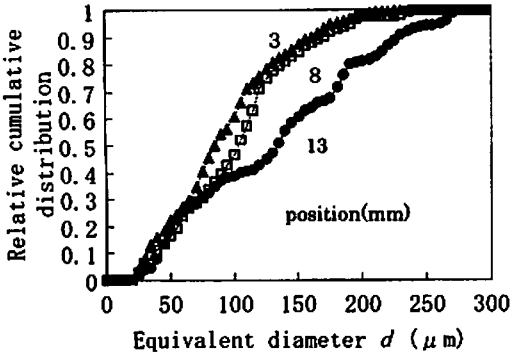

Fig. 7. Relative cumulative distribution of ice crystal diameter at T_{cp} −40 °C.

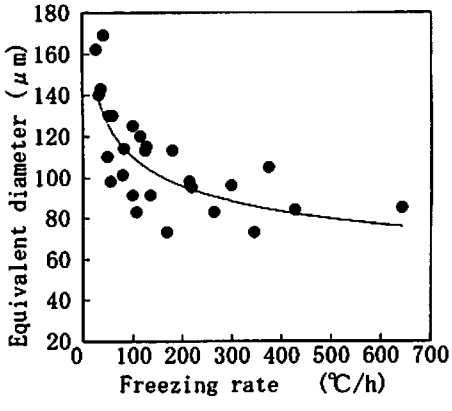

Fig. 8. Ice crystal diameter according to the freezing rate. Experimental data: (●) and fitting curve (−).

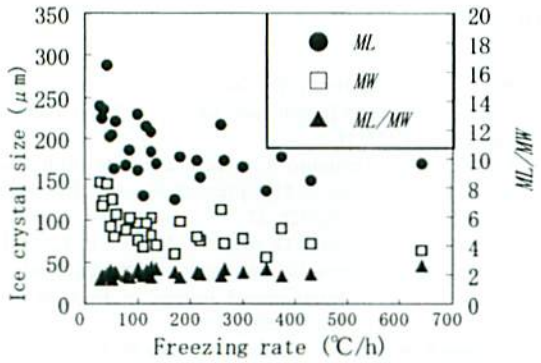

Fig. 9. The effect of the freezing rate on ice crystal size and *ML/MW*.

the values of freezing time and the freezing rate were 22.8×10^{-3} h and 219.5 °C/h, respectively. Fig. 6(a) and (b) shows the cross-sectional images of ice crystals at T_{cp} −30 °C and −190 °C, respectively. These images clearly show the ice crystals and concentrated Rhodamine B; the former was distinguished by a dark color, while the latter turns out white. These results demonstrated that MSIPS allowed observation of ice crystals directly in a frozen dilute solution.

A series of 200 cross-sectional images 1 mm in height was analyzed to investigate the distribution of ice crystal size. Fig. 7 shows a relative cumulative distribution of the equivalent diameters of ice crystals at −40 °C. These curves were obtained at locations of 3, 8 and 13 mm from the bottom surface, and the number of ice crystals counted were 3667, 2492, and 1497, respectively. The equivalent diameters were increased according to the distance of the ice crystals from the bottom surface.

The equivalent diameter according to freezing rate is plotted in Fig. 8, which was obtained by pooling all the results. The equivalent diameter of ice crystals were in the range of 85–169 μm, and then decreased exponentially in increasing freezing rate at T_{cp} −20 to −80 °C. The ratio of mean major length (*ML*) to mean minor width (*MW*) *was* calculated for obtaining a quantitative index of morphology. As the ratio approaches close to unity, morphology can be regarded as circular or cubic. On the other hand, it would be ellipse or rectangular, if the ratio was far different from unity. As shown in Fig. 9 the values of *ML* and *MW* also decreased in increasing the freezing rate and the ratio (*ML/MW*) was in the range of 2.0±0.5, indicating no significant dependence of freezing rate on ice crystal morphology.

Fig. 10 shows the 3-D ice crystal morphology at T_{cp} −120 °C. The scales of the image were 678 μm in length, 473 μm in width and 1000 μm in height, respectively. Arbitrary cross-section of ice crystal is also shown. Fig. 11 shows a 3-D image of the labeled ice columns and three, extracted ice columns at 8 mm from cooling plate at T_{cp} −40 °C. The scales of the image were 700 μm in length, 530 μm in width and 1000 μm in height, respectively.

The 3-D morphology of ice crystals was found to form a bundle of continuous columns or dendrite columns at any freezing conditions. The volume distribution of the ice columns at T_{cp} −40 °C was calculated from labeled ice columns shown in Fig. 11. The ice columns summed up to 2.6×10^{8} μm^3, which was 69% of the whole observed volume, 3.7×10^{8} μm^3. As shown in Fig. 12, the volume of ice crystals were in the range of 4.6×10^{4}–3.3×10^{7} μm^3, and 36 ice columns were counted in the 3-D image.

The proposed method using the MSIPS has demonstrated various advantages comparing with conventional observation techniques and also provided a new tool to investigate quantitatively the relationships between freezing conditions and characteristics of ice crystals such as morphology, size and distribution.

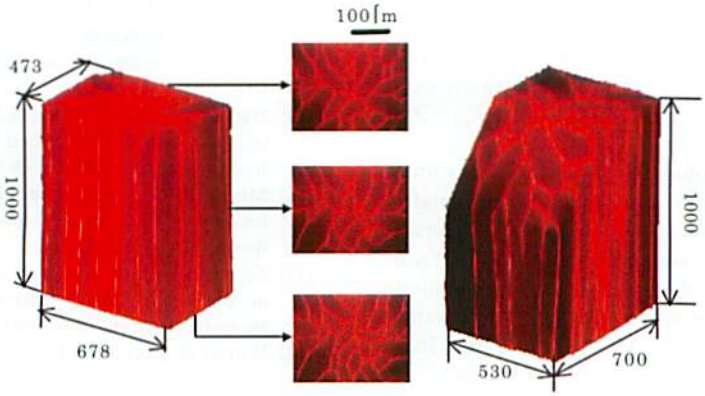

Fig. 10. 3-D image of ice crystal and arbitrary cross-section image at T_{cp} −120°C.

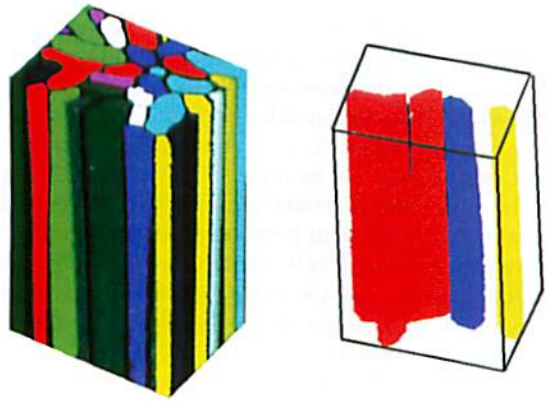

Fig. 11. 3-D image of labeled ice columns at 8 mm from cooling surface (at T_{cp} −40 °C).

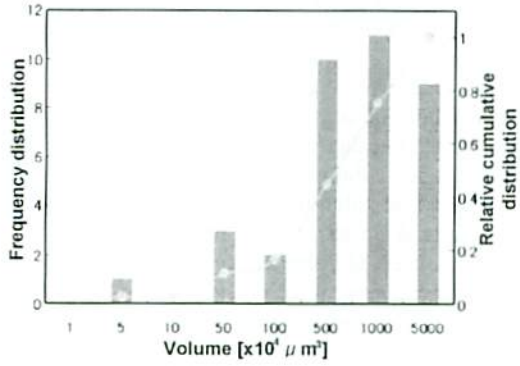

Fig. 12. The volume distribution of ice columns (at T_{cp} −40 °C).

4. Conclusions

The 3-D morphology and distribution of ice crystals in a frozen dilute solution with agar was analyzed with the Micro-Slicer Image Processing System (MSIPS).

1. The equivalent diameter of ice crystals were in the range of 73–169 μm, and decreased exponentially in increasing freezing rate at T_{cp} −20 to −80 °C.
2. The 3-D morphology of ice crystals was found to form a bundle of continuous or dendrite columns at any our experimental conditions.
3. The ice columns summed up to 2.6×10^8 μm³, which was 69% of the whole-observed volume, 3.3×10^7 μm³. The volume of ice crystals were in the range of 4.6×10^4–3.7×10^8 μm³, and 36 ice columns were counted in the 3-D image.
4. MSIPS allowed observation of ice crystals directly in a frozen dilute solution.

References

[1] Bevilacqua A, Zertizky E, Calvelo A. Histological measurements of ice in frozen beef. Journal of Food Technology 1979;14:237–51.
[2] Fuchigami M, Teramoto A. Structural and textural changes in kinu-tofu due to high-pressure-freezing. Journal of Food Science 1997;62:828–32.
[3] Monica T, Kalichevsky D, Ablett S, Lillford P, Knorr D. Effects of pressure-shift freezing and conventional on model food gels. International Journal of Food Science and Technology 2000;35:163–72.
[4] Bolliger S, Wildmoser H, Goff D, Tharp W. Relationships between ice cream mix viscoelasticity and ice crystal growth in ice cream. International Dairy Journal 2000;10:791–7.
[5] Sagara Y. Structural models related to transport properties for the dried layer of food materials undergoing freeze-drying. Drying Technology 2001;19:281–96.
[6] Araki T, Sagara Y, Abdullah K, Tambunan H. Transport properties of cellular food materials undergoing freeze-drying. Drying Technology 2001;19:297–312.
[7] Russell B, Cheney E, Wantling D. Influence of freezing conditions on ice crystallization in ice cream. Journal of Food Engineering 1999;39:179–91.
[8] Donhowe R, Hartel W, Bradley L. Determination of ice crystal size distribution in frozen desserts. Journal of Dairy Science 1991;74:3334–44.
[9] Kojima T, Oguri N, Shimada K, Souzu H. Cryomicroscopic observation of ice crystal gemination initiated by silver iodide-alginate gel droplets in various solutions. Cryo-letters 1988;9:348–55.
[10] Williamson A, Lips A, Clark A, Hall D. Ripening of faceted ice crystals. Powder Technology 2001;121:74–80.
[11] Evans J, Adler J, Mitchell J, Blanshard J, Rodger G. Use of confocal laser scanning microscope in order to observe dynamically the freeze–thaw cycle in an autoflorescent substance and to measure ice crystal size in situ. Cryobiology 1996;33:27–33.
[12] Bevilacqua A, Zartizky NE. Ice morphology in frozen beef. Journal of Food Technology 1980;15:589–97.
[13] Martino N, Zaritzky E. Ice crystal size modification during frozen beef storage. Journal of Food Science 1998;53:1631–7.
[14] Martino N, Otero L, Sanz D, Zaritzky E. Size and location of ice crystals in pork frozen by high-pressure-assisted freezing as compared to classical methods. Meat Science 1998;50:303–13.
[15] Hagiwara T, Wang H, Suzuki T, Takai R. Fractal analysis of ice crystals in frozen food. Journal of Agricultural and Food Chemistry 2002;50:3085–9.
[16] Miyawaki O, Abe T, Yano T. Freezing and ice structure formed in protein gels. Bioscience Biotechnology and Biochemistry 1992;56:953–7.
[17] Seoung-Kwon B, Miyawaki O, Yano T. Ice structure size in frozen agar gels by mercury poromsimetry. Bioscience Biotechnology and Biochemistry 1993;57:1624–7.
[18] Woinet B, Andrieu J, Laurent M. Experimental and theoretical study of model food freezing. Part 1. Heat transfer modelling. Journal of Food Engineering 1998;35:381–94.
[19] Woinet B, Andrieu J, Laurent M, Min G. Experimental

and theoretical study of model food freezing. Part 2. Characterization and modeling of ice crystal size. Journal of Food Engineering 1998;35:395–407.

[20] Chevalier D, Bali A, Ghoul M. Freezing and ice crystal formed in a cylindrical food model: part 1. Freezing at atmospheric pressure. Journal of Food Engineering 2000; 46:277–85.

[21] Faydi E, Andrieu J, Laurent P. Experimental study and modeling of the ice crystal morphology of model standard ice cream. Part 1, direct characterization method and experimental data. Journal of Food Engineering 2001;48: 283–93.

[22] Kobayashi K, Higuchi T, Aoki I, Kudoh K. Development of microslicer implementation of 3-dimensional internal structure (in Japanese). Journal of the Japan Society for Precision Engineering 1995;61:100–4.

[23] Do G, Sagara Y, Kudoh K, Yokota H, Higuchi T. Surface area and volume measurements of a broccoli (*Brassica oleracea* L.var.italica PLEN) with a microslicer-image data processing system (in Japanese). Journal of the Society of Agricultural Structures 1997;28:21–9.

[24] Yokota H, Kudoh K, Higuchi T, Sagara Y, Do G. Observation and measurement of frozen biological sample by 3-dimensonal internal structure microscope (in Japanese). Cryobiology and Cryotechnology 1998;44:1–9.

[25] Kimura J, Tsukise A, Yokota H, Nambo Y, Higuchi T. The application of three-dimensional internal structure microscopy in the observation of mare ovary. Anatomia Histrogia Embryologia 2001;30:309–12.

[26] Ogawa Y, Sugiyama J, Kuensting H, Ohtani T, Hagiwara S, Liu X, et al. Advanced technique for three-dimensional visualization of compound distribution in a rice kernel. Journal of Agricultural and Food Chemistry 2001;49:736–40.

[27] Do G, Sagara Y, Tabata M, Kudoh K, Higuchi T. Three-dimensional measurement of ice crystals in frozen beef with micro-slicer image processing system. International Journal of Refrigeration [in press].